CHAPTER 2

Understanding the Chemistry of Photocatalytic Processes

AMER HAKKI*[a], JENNY SCHNEIDER[b], AND DETLEF BAHNEMANN[b,c]

[a]Department of Chemistry, King's College, University of Aberdeen, Aberdeen AB24 3UE, UK; [b]Institut für Technische Chemie, Leibniz Universität Hannover, Callinstrasse 3, D-30167, Hannover, Germany; [c]Laboratory for Nanocomposite Materials, Department of Photonics, Faculty of Physics, Saint-Petersburg State University, Ulianovskaia str. 3, Peterhof, Saint-Petersburg, 198504, Russia
*E-mail: a.hakki@abdn.ac.uk

2.1 Thermodynamic Constraints for Photocatalytic Processes

The attainable oxidation and reduction half-reactions that can be achieved on the surface of a given semiconductor photocatalyst are limited by the positions of the band edges of the photocatalyst.[1]

It is well known that different semiconductors may have significantly different conduction and valence band edges. The potential of these edges will determine the thermodynamic feasibility of the reactions that can proceed. Figure 2.1 shows the CB and VB potentials of various semiconductors.

In this respect, it is essential to take into account the reduction potentials (E) of the substrate, as well as those of the intermediates that are formed during

RSC Energy and Environment Series No. 14
Photocatalysis: Fundamentals and Perspectives
Edited by Jenny Schneider, Detlef Bahnemann, Jinhua Ye, Gianluca Li Puma, and Dionysios D. Dionysiou

Published by the Royal Society of Chemistry, www.rsc.org

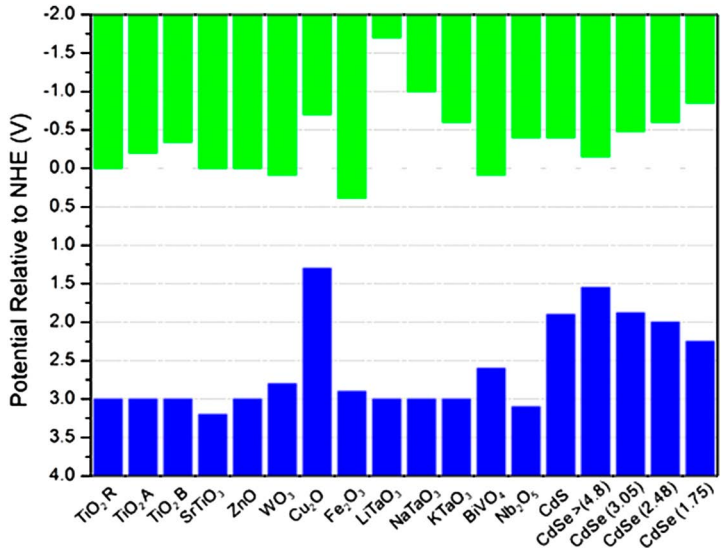

Figure 2.1 Bandgap energies of different semiconductors and respective band edge positions, *i.e.*, valence band (blue columns) and conduction band (green columns) energies, relative to the normal hydrogen electrode (NHE) at pH 0. The values of TiO_2 were obtained from ref. 2. R, A, and B refer to rutile, anatase, and brookite, respectively. The values of $MTaO_3$ (M = Li, Na or K) were obtained from ref. 3. The values of CdSe were estimated from ref. 4 and all other values were obtained from ref. 5.

the photocatalytic reaction(s). However, the reduction potentials for different organic or inorganic compounds are usually dependent on the reaction conditions such as pH and the employed electrolyte. The reduction potential of the couples $M/M^{\bullet -}$ refer to reactions described by eqn (2.1) and (2.2):

$$\text{oxidant} + e^- \rightarrow \text{reductant}\ (e.g.\ Cl^{\bullet}/Cl^-) \tag{2.1}$$

$$\text{oxidant} + e^- + nH^+ \rightarrow \text{reductant}\ (e.g.\ {}^{\bullet}OH, H^+/H_2O) \tag{2.2}$$

These reactions refer to one-electron reduction reactions the potentials of which are given *versus* the standard hydrogen electrode (SHE). Table 2.1 includes the reduction potentials of the most important inorganic species that may be present in photocatalytic systems.

Substrates M with more positive reduction potentials are stronger oxidants than those exhibiting lower or negative reduction potentials. Thus, as long as the reduction potential of the donor is less positive than the valence band edge and the reduction potential of the acceptor is less negative than the conduction band edge (Figure 2.2), the electron transfer will be thermodynamically favorable. For example, water [$E({}^{\bullet}OH, H^+/H_2O) = 2.59$ V] or carbonate ion [$E(CO_3^{2-}/CO_3^{\bullet -}) = 1.5$ V] can theoretically be oxidized to hydroxyl radical or carbonate radical anions, respectively, by photogenerated holes of TiO_2. On the other hand, Fe^{3+} ions [$E(Fe^{3+}/Fe^{2+}) = 0.77$ V] or Ag^+ ions

Table 2.1 Reduction potentials of some species that may be involved in photocatalytic systems.

Reduction reaction	E^a (V)	Remark
$aq + e^- \rightarrow e_{aq}^-$	−2.870	
$Br^\bullet + e^- \rightarrow Br^-$	2.000	
$CN^\bullet + e^- \rightarrow CN^-$	1.900	
$CO_2 + e^- \rightarrow CO_2^{\bullet-}$	−1.900	
$CO_3^{\bullet-} + e^- \rightarrow CO_3^{2-}$	1.500	
$CO_2^{\bullet-} + H^+ + e^- \rightarrow HCO_3^-$	1.070	pH 7
$Cl^\bullet + e^- \rightarrow Cl^-$	2.200–2.600	
$Cl_2 + e^- \rightarrow Cl_2^{\bullet-}$	0.420–0.600	
$Cl_2^{\bullet-} + e^- \rightarrow 2Cl^-$	2.300	
$F^\bullet + e^- \rightarrow F^-$	3.600	
$I^\bullet + e^- \rightarrow I^-$	1.270–1.420	
$I_2^{\bullet-} + e^- \rightarrow 2I^-$	1.000–1.130	
$I_2 + e^- \rightarrow I_2^{\bullet-}$	0.420–0.600	
$^\bullet NO_2 + e^- \rightarrow NO_2^-$	0.870–1.040	
$^\bullet NO_3 + e^- \rightarrow NO_3^-$	2.300–2.600	
$^\bullet OH + H^+ + e^- \rightarrow H_2O$	2.590–2.850	pH 0
	1.800–2.180	pH 7
$^\bullet OH + e^- \rightarrow OH^-$	1.900	
$O_2 + e^- \rightarrow O_2^{\bullet-}$	−0.330	
$O_2 + H^+ + e^- \rightarrow HO_2^\bullet$	−0.037	pH 0
$O_2^{\bullet-} + H^+ + e^- \rightarrow HO_2^-$	1.000	
$O_2^{\bullet-} + 2H^+ + e^- \rightarrow H_2O_2$	0.940	pH 7
$HO_2^\bullet + H^+ + e^- \rightarrow H_2O_2$	1.420	pH 0
$HO_2^\bullet + e^- \rightarrow HO_2^-$	0.790	
$H_2O_2 + H^+ + e^- \rightarrow H_2O + {}^\bullet OH$	0.800	pH 7
$O_3 + e^- \rightarrow O_3^{\bullet-}$	1.190–1.600	pH > 11
$O_3 + H^+ + e^- \rightarrow HO_3^\bullet$	1.800	pH 7
$HS^\bullet + e^- \rightarrow HS^-$	1.150	
$^\bullet SO_3^- + e^- \rightarrow SO_3^{2-}$	0.630	pH > 8
$SO_4^{2-} + H_2O + e^- \rightarrow {}^\bullet SO_3^- + 2OH^-$	−2.470	
$SO_4^{\bullet-} + e^- \rightarrow SO_4^{2-}$	2.430	
$Fe^{3+} + e^- \rightarrow Fe^{2+}$	0.770	
$Ag^+ + e^- \rightarrow Ag$	0.800	

[a]Reduction potential referring to one-electron reduction *vs.* SHE. In the case of proton involvement, *E* values may be used to estimate the standard potentials E° as defined by the Nernst equation. Data are taken from ref. 6.

[$E(Ag^+/Ag) = 0.8$ V] can be reduced by the photogenerated conduction band electrons in TiO_2. Notably, the absolute position of the bands of metal oxide photocatalysts exhibit a Nernstian shift with the change of pH (−0.059 V per pH unit). Since most of the one-electron redox reactions listed in Table 2.1 also exhibit such Nernstian behavior, the chosen pH values usually do not play a significant role.

Moreover, it is in fact critical to provide an overpotential for each process, to initiate and subsequently drive the electron transfer process. Without an overpotential, even a good photocatalyst cannot ensure a sufficient high rate of reaction.[7]

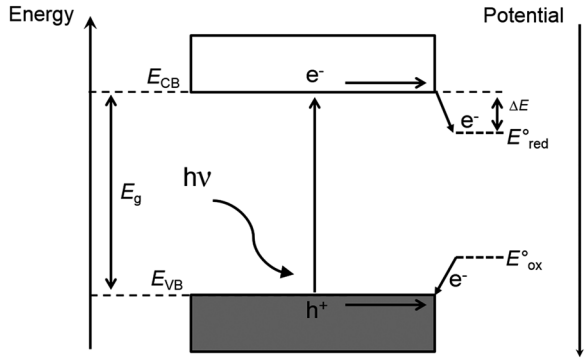

Figure 2.2 Thermodynamic constraints on the transfer of charge carriers to adsorbed molecules; ΔE represents the kinetic overpotential of the reduction process. (Adapted with permission from ref. 7. Copyright 2013 Wiley-VCH Verlag GmbH, Weinheim.)

Nevertheless, besides the band alignment of a semiconductor relative to the redox potentials of the substrate it is important to consider its stability, *e.g.*, in aqueous solutions, where most photocatalytic reactions are performed. While most semiconductors are chemically quite stable in aqueous environment, oxidative and/or reductive photocorrosion processes are often encountered upon band gap illumination. Chen *et al.*[8] introduced an approach to calculate the thermodynamic oxidation potential (φ^{ox}) and reduction potentials (φ^{re}) of semiconductors in aqueous solution. In the following, ZnS is taken as an example to introduce the details of such a calculation. The φ^{ox} and φ^{re} for ZnS can be defined according to eqn (2.3) and (2.4):

$$ZnS + 2h^+ + H_2O \leftrightarrow ZnO + S + 2H^+ \text{ (oxidation)} \quad (2.3)$$

$$ZnS + 2e^- + 2H^+ \leftrightarrow Zn + H_2S \text{ (reduction)} \quad (2.4)$$

as follows:

$$\varphi^{ox} = [G(ZnO) + G(S) + 2G(H^+) - G(ZnS) - G(H_2O)]/2eF \quad (2.5)$$

$$\varphi^{re} = [G(Zn) + G(H_2S) - G(ZnS) - G(H^+)]/2eF \quad (2.6)$$

Cases in which the half reactions are unknown or the Gibbs free energy for the compound is not given are also discussed in detail in ref. 8. Figure 2.3 shows the calculated φ^{ox} and φ^{re} for five selected classes of semiconductors (metal oxides, oxynitrides, groups III–V and groups II–IV like compounds, and group IV like elemental semiconductors) as well as the water redox potentials ($\varphi(O_2/H_2O)$ and $\varphi(H^+/H_2)$) and the valence and conduction band edges relative to the NHE potential and to the vacuum level. According to this figure, if the conduction band edge and φ^{re} of a semiconductor are both higher than $\varphi(H^+/H_2)$, the semiconductor can be a stable photocathode against reduction; and if valence band edge and φ^{ox} are both lower than $\varphi(O_2/H_2O)$, the semiconductor can be a stable photoanode against oxidation.

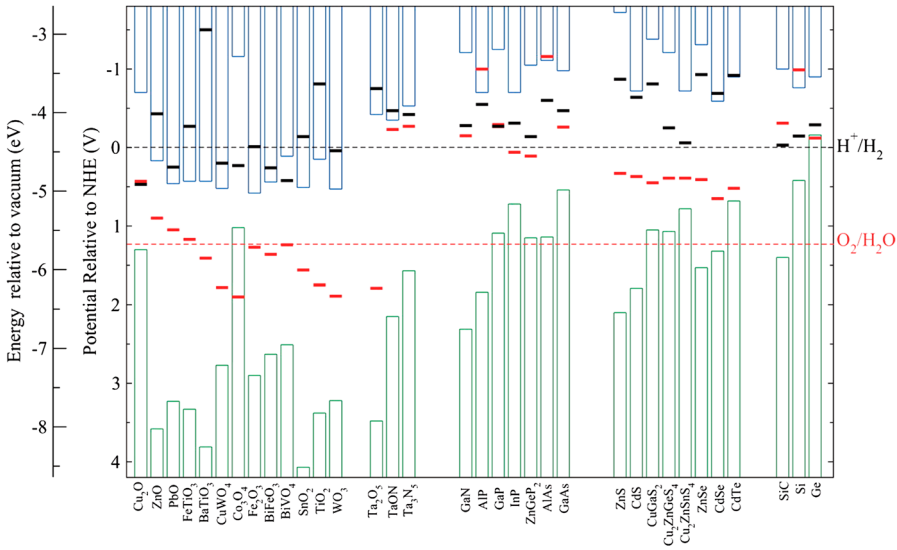

Figure 2.3 Calculated oxidation potentials φ^{ox} (red bars) and reduction potentials φ^{re} (black bars) relative to NHE and vacuum level for a series of semiconductors in solution at pH 0, ambient temperature (298.15 K), and pressure (1 bar). The water redox potential φ (O_2/H_2O) and φ (H^+/H_2) (dashed lines) and the valence (green columns) and conduction (blue columns) band edge positions at pH 0 are also plotted. (Reprinted with permission from ref. 8. Copyright 2012 American Chemical Society.)

However, the calculation method proposed by Chen *et al.*[8] is not necessarily accurate for metal oxides, since in such cases reactions with other species rather than with water is considered, as shown, for example, for TiO_2:

$$TiO_2 + 4H^+ + 2Cl^- \leftrightarrow TiCl_4 + 2H_2 + O_2 \quad (\varphi^{ox} = 1.75 \textit{ vs.} \text{ NHE}) \qquad (2.7)$$

This reaction is valid only for chloride containing metal oxide semiconductors, such as TiO_2 Evonik P25. In the absence of chloride or of any others inorganic species TiO_2 can react just with water. In such a case TiO_2 will be oxidized by photogenerated holes resulting in the formation of oxygen vacancies. Those vacancies formed at the surface can be "repaired" by reaction with water. Similar processes have already been proposed by different research groups[9–15] for photocatalytic gas phase reactions and by Montoya *et al.*[16,17] for photo-oxidation processes at the liquid–solid interface. The general mechanism of the later process is shown in Figure 2.4. It involves three reaction steps: (1) oxidation of the TiO_2 surface by hole trapping at surface lattice oxygen atoms resulting in the formation of terminal oxygen radicals, which are able to react with dissolved substrate species; (2) the incorporation of these terminal oxygen radicals into photo-oxidation products with the simultaneous generation of TiO_2 surface oxygen vacancies; (3) the dissociative adsorption of H_2O molecules into the terminal oxygen vacancies resulting in the "healing" of the catalyst surface.

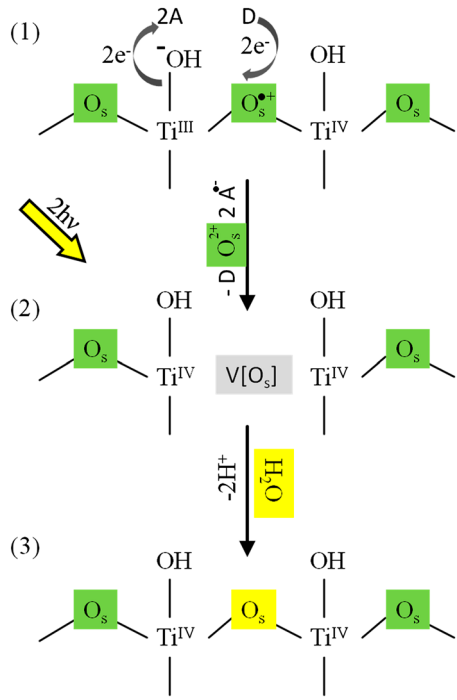

Figure 2.4 Photocatalytic oxidation processes under active participation of the surface lattice oxygen atoms leading to reconstruction of the TiO_2 surface. (Reprinted with permission from ref. 18. Copyright 2014 American Chemical Society.)

According to the above-discussed cases, controlling the band edge potentials is an essential issue to be considered when developing photocatalytic materials with respect to their desired application. The band levels can be adjusted by controlling the particle size of the employed photocatalyst. When the crystallite dimension of a semiconductor particle falls below a critical radius, usually less than 10 nm for metal oxides, the charge carriers appear to behave like the energy levels of a "particle in the box". Thus, the apparent bandgap increases and the band edges E_{CB} and E_{VB} shift negatively and positively, respectively, to yield larger redox potentials. For example, Kormann *et al.*[19] have reported a redshift in the spectra of TiO_2 nanoparticles during their growth up to $d < 3$ nm. As a result of the shift of the band edges, the use of size quantized semiconductor particles may result in increased photoefficiencies for systems in which the rate-limiting step is the charge transfer. However, in some cases the photo-efficiencies were even found to decrease as the particle size decreased due to an increased number of surface defects.[20]

The band levels, especially the conduction band edge, also depend on the crystallite phase of a given semiconductor. In the case of TiO_2, for example, the flat band potential of brookite nanorods has been found to be shifted by 140 mV more cathodically than the flat band potential of anatase nanoparticles,[2] whereas the flat band potential of rutile has been reported to be

shifted by 200 mV more anodically than that of anatase (*cf.* Figure 2.1). The potential of the valence band edges is usually calculated by subtraction of the energy gaps of the semiconductor (obtained from diffuse reflectance measurements) from the conduction band energy (obtained, for example, by impedance spectroscopy) assuming that the flat band potential is equal to the potential of the conduction band edge. In case of TiO_2, for example, the valence band edges have been reported to be almost constant at 3.0 V *vs.* NHE at pH 0 regardless of the crystalline phase, anatase, rutile, or brookite, whereas their band gap energies are 3.2, 3.0, and 3.3 eV, respectively.

2.2 Single and Multiple Electron Transfer Reactions

In most cases, the photocatalytic transformation of the educts to the final products needs more than one-electron transfer reaction, which may occur either as sequential single-electron processes or through the simultaneous transfer of several accumulated electrons. In the case of carbon dioxide, for example, the multistep reduction involves up to eight electrons and protons, cleavage of C–O bonds, and formation of C–H bonds, and may lead to several different products depending on the specific reaction pathway. The single-electron reduction of CO_2 to the anion radical $CO_2^{\bullet-}$ (eqn (2.8)) has a strongly negative electrochemical potential of −1.9 V *versus* the normal hydrogen electrode (NHE):

$$CO_2 + e^- \rightarrow CO_2^{\bullet-} \quad (E^0_{redox} = -1.90\ V) \tag{2.8}$$

In fact, very few semiconductors provide sufficient potential to transfer a single photogenerated electron to a free CO_2 molecule, making this step highly improbable.

However, the situation is better for the proton-assisted transfer of multiple electrons. Eqn (2.9)–(2.14) show the reactions of the transfer of two to eight electrons, and a corresponding number of protons, to CO_2 to form formic acid, carbon monoxide, formaldehyde, methanol, and methane, respectively. As can be seen from the electrochemical reduction potentials (*versus* NHE at pH 7), all these potentials are less negative than the conduction band edges of many semiconductors, including TiO_2[7] (Figure 2.1):

$$CO_2 + 2H^+ + 2e^- \rightarrow HCOOH \quad (E^0_{redox} = -0.61\ V) \tag{2.9}$$

$$CO_2 + 2H^+ + 2e^- \rightarrow CO + H_2O \quad (E^0_{redox} = -0.53\ V) \tag{2.10}$$

$$CO_2 + 4H^+ + 4e^- \rightarrow HCHO + H_2O \quad (E^0_{redox} = -0.48\ V) \tag{2.11}$$

$$CO_2 + 6H^+ + 6e^- \rightarrow CH_3OH + H_2O \quad (E^0_{redox} = -0.38\ V) \tag{2.12}$$

$$CO_2 + 8H^+ + 8e^- \rightarrow CH_4 + 2H_2O \quad (E^0_{redox} = -0.24\ V) \tag{2.13}$$

$$2H^+ + 2e^- \rightarrow H_2 \quad (E^0_{redox} = -0.41\ V) \tag{2.14}$$

However, in the literature, there is little evidence of such concerted multielectron transfer processes in the absence of any co-catalyst.[7,18] Hence, on the bare photocatalyst surface the reaction is likely to proceed through a series of one-electron transfer steps with the first electron transfer remaining a severe obstacle to the photoreduction of CO_2, thus constituting a strongly limiting

case.[21] Moreover, such multi-electron steps must overcome some additional requirements. Recently, Ramesha *et al.*[21] have reported that the one-electron reduction of CO_2 employing a TiO_2 cathode in acetonitrile proceeds at an onset potential of −0.95 V (*vs.* NHE), which is significantly lower than the one observed with a glassy carbon electrode, indicating an electrocatalytic role of TiO_2. The authors attributed this electrocatalytic activity of TiO_2 films to the binding of CO_2 to Ti^{3+} sites, formed *via* the reduction of Ti^{4+} sites at potentials more negative than −0.95 V *versus* NHE. Similar phenomena may also occur upon illumination of TiO_2, for which the formation of Ti^{3+} sites is well known.

Another important factor that has to be considered here is that the reported redox potentials in most cases (*cf.* Table 2.1) refer to free species in solutions. However, in the case of photocatalytic reactions, the molecule of interest usually has to be adsorbed on the surface of the solid photocatalyst to be reduced or oxidized. Thus, a change of its redox properties upon its interaction with the surface can be expected. Zapol and co-workers, for example, predicted *via* their calculations a decrease in the reduction potential of adsorbed CO_2 on the (101) surface of TiO_2 by 0.24 V as compared to the reduction potential of a CO_2 molecule in aqueous solution.[22] This lowering of the reduction potential can be attributed to the monodentate and bidentate configuration of CO_2 formed on the TiO_2 surface, which in turn facilitates the charge transfer through hybridized orbitals.[23]

Another example of a multi-electron reduction is the photocatalytic reduction of O_2 over WO_3 to produce H_2O_2. The conduction band minimum of WO_3 (*ca.* +0.5 V *vs.* NHE) is much lower than the potentials of O_2 reduction *via* the one-electron process (Table 2.1). However, the multi-electron reduction of O_2 [$O_2 + 2e^- + 2H^+ \rightarrow H_2O_2$, $E^\circ(O_2/H_2O_2) = +0.68$ V; or $O_2 + 4e^- + 4H^+ \rightarrow 2H_2O$, $E^\circ(O_2/H_2O) = +1.23$ V *vs.* SHE] is able to proceed thermodynamically, even by the photoexcited electrons generated in the conduction band of WO_3.[24] Such multi-electron transfer reactions can be enhanced by the presence of metal nanoparticles, as co-catalysts, *e.g.* Pt, on the surface of the metal oxide photocatalyst acting as a pool on which the electrons are accumulated before they are transferred to the adsorbed substrate.[24]

When discussing single or multiple electron transfer processes the photocatalytic water oxidation has to be taken into account. Very often the redox potential of +1.23 V *vs.* SHE for water oxidation is considered for the evaluation of a semiconductor as a suitable photoanode. This redox potential of +1.23 V requires that four electrons are simultaneously transferred from at least two adsorbed water molecules to the semiconductor. However, in the absence of a co-catalyst, where the charges can be accumulated, this four-electron transfer process is most unlikely. The single electron oxidation of water proceeds *via* the following reactions:

$$H_2O + h^+ \rightarrow {}^{\bullet}OH + H^+ \xrightarrow{{}^{\bullet}OH/H^+} H_2O_2 \quad (E^0 = 2.3\ vs.\ \text{SHE}) \tag{2.15}$$

$$H_2O_2 + h^+ \rightarrow O_2^{\bullet -} + 2H^+ \quad (E^0 = 1.3\ vs.\ \text{SHE}) \tag{2.16}$$

$$O_2^{\bullet -} + h^+ \rightarrow O_2 \quad (E^0 = -0.08\ vs.\ \text{SHE}) \tag{2.17}$$

Obviously, the first oxidation step of water forming $^{\bullet}OH$ radicals is thermodynamically the most difficult step. Moreover, according to the oxidation potential of TiO_2 shown in Figure 2.3 the photogenerated holes will oxidize the semiconductor's surface first, forming $O^{\bullet-}$, generating hydroxyl radicals from water. This conclusion is supported by many reports, which clearly show that the primary products of the hole oxidation are not superficially bound or free $^{\bullet}OH$ radicals but rather $O^{\bullet-}$ radical ions in the TiO_2 lattice.[25–28] For example, Imanishi *et al.* estimated the energy levels of O 2p orbitals for H_2O and ^{-}OH from the reported photoelectron emission spectra and for Ti–OH at the TiO_2/water interface from UV photoelectron spectra.[29–31] Based on these results the effective O 2p levels were found to be far below the valence band of TiO_2, thus water oxidation to $^{\bullet}OH$ radicals through the photogenerated holes was excluded. Hence, the mechanism of photocatalytic water oxidation proposed here proceeds *via* photocorrosion of the semiconductor resulting in the release of oxygen from the lattice, while the formed oxygen vacancies will be healed by the subsequent adsorption of a water molecule. A similar mechanism for O_2 formation employing TiO_2 photocatalysis had already been proposed by Salvador.[32]

2.3 Role of the Substrate Structure in the Photocatalytic Process

The nature of the substrate to be photocatalytically converted strongly affects the overall chemistry of a photocatalytic system through one, or more, of the following processes:

(i) The formation of a solid–substrate complex upon adsorption of the substrate on the surface of the photocatalyst may play an important role. The thus formed complex will have its own chemistry that differs from that of both of its components. Moreover, the formation of this complex may also change the charge carrier formation pathway, provided that this complex also absorbs light,[33] as well as the activation energy of the photo(catalytic) system. A wide variety of organic or inorganic compounds (that do not absorb visible light) can form surface complexes with TiO_2 (or other wide bandgap semiconductors) thus introducing new absorbance bands resulting a redshift of the semiconductor's absorption compared to the unmodified one (Figure 2.5).[34] This is different from the case of the well-known dye sensitization where the sensitizer itself absorbs the activating light.[35] The optical absorption of the thus formed complexes is usually influenced by the properties of both the semiconductor and the ligands.

(ii) The structure of the substrate may affect the formation as well as the fate of the photocatalytically produced reactive oxygen species. For example, H_2O_2 evolution is found to be much lower during the photocatalytic degradation of aromatic substrates such as benzoic acid (BA)

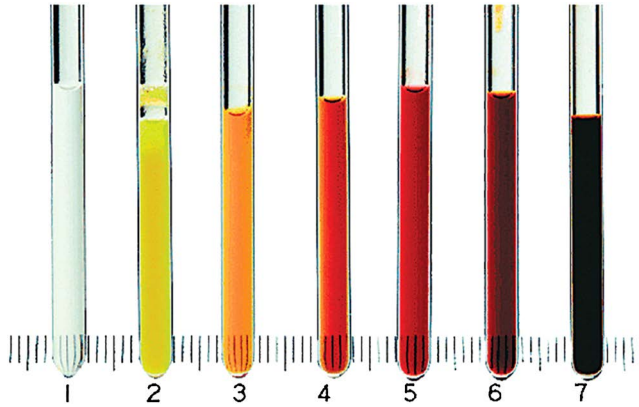

Figure 2.5 Surface-modified 45 Å TiO_2 nanoparticles with different bidentate ligands: (1) bare TiO_2, (2) salicylic acid, (3) dihydroxycyclobutenedione, (4) vitamin C, (5) alizarin, (6) dopamine, and (7) *tert*-butyl catechol. (Reprinted with permission from ref. 34. Copyright 2002 American Chemical Society.)

and the azo dye acid red 1 (AR1) than its evolution reported during the photocatalytic formic acid degradation on the same fluorinated TiO_2.[36] The presence of fluoride anions on the TiO_2 surface has a shielding effect on the photocatalytic degradation of hydrogen peroxide occurring at the water–semiconductor interface. In the case of the photocatalytic oxidation of formic acid (*cf.* eqn (2.18)), a strongly reducing species, *i.e.*, $CO_2^{\bullet-}$ (or $HCO_2^{\bullet}$ depending on the pH, with a pK_a of 1.4), is formed. In fact, its redox potential, *i.e.*, $E^{\circ}(CO_2/CO_2^{\bullet-}) = -1.9$ V, makes the carbon dioxide radical anion able to inject an electron into the conduction band of titanium dioxide, *i.e.*, the so-called current doubling effect, see reaction (eqn (2.19)), and also to mediate the reduction of a wide variety of molecules, in particular dissolved O_2, according to reaction (2.20):

$$HCO_2^- + h^+ \rightarrow CO_2^{\bullet-} + H^+_{aq} \quad (2.18)$$

$$CO_2^{\bullet-} \rightarrow CO_2 + e^-_{CB} \quad (2.19)$$

$$CO_2^{\bullet-} + O_2 \rightarrow CO_2 + O_2^{\bullet-} \quad (2.20)$$

In both cases, the carbon dioxide radical anion plays a major role in the production of H_2O_2 over fluorinated TiO_2. The one-electron oxidation of BA and AR1, however, does not produce strongly reducing free radical intermediates, thus explaining the overall lower yield observed for these compounds.

Moreover, the addition of oxalic acid as a hole scavenger has been found to significantly accelerate the reductive photocatalytic decomposition of perfluorooctanoic acid (PFOA) under inert atmosphere employing TiO_2 under 254 nm UV illumination. The ESR analysis as well as the analysis of the formed intermediates indicate that this enhancement is due to the formation of

$CO_2^{\bullet-}$, which is produced through the reaction between oxalic acid and photogenerated holes, in the photocatalytic PFOA decomposition.[37]

Schwitzgebel *et al.*[38] have also shown that the photocatalytic degradation pathway is influenced by the structure of the reactant. They have reported that the photocatalytic oxidation of aliphatic reactants including a hydrocarbon, an alcohol, a ketone, and a carboxylic acid occurs not only *via* the photogenerated holes but also *via* the photogenerated electrons. The superoxide radical formed as a result of the reduction of O_2 by conduction band electrons participates in oxidation reactions whereas electrons do not participate in the initiation or propagation of the particularly efficient oxidation of an aliphatic aldehyde (discussed in more detail in Section 2.4).

(iii) In some cases the substrate itself plays the role of a recombination center *via* an electron shuttle mechanism (Z scheme deactivation mechanism). For example, hydroquinone (HQ) and benzoquinone (BQ) are common intermediates usually identified when a benzene-ring-containing substrate is photocatalytically degraded. Flash photolysis experiments have shown that BQ produced directly during photocatalytic degradation of 4-chlorophenol (4-CP) is one of the first oxidation products.[39] Richard[40] has shown that BQ can act as a very effective electron scavenger over illuminated TiO_2 or ZnO and is able to compete successfully with molecular oxygen for the photogenerated conduction band electrons of the semiconductor particle, producing HQ. Thus, both HQ and BQ together may constitute a photocatalytic "balance", which is attributed to a fast electron shuttle mechanism (Scheme 2.1). This "equilibrium" between HQ and BQ acts as a photocatalytic short circuit resulting in an external recombination and thus a lowering of the photonic efficiency for the photocatalytic degradation of aromatic compounds such as phenol or 4-chlorophenol.[39]

Moreover, BQ can also be oxidized (by the attack of a hydroxyl radical) to hydroxybenzoquinone (HBQ), which again contributes to the so-called electron shuttle mechanism *via* the formation of hydroxyhydroquinone (HHQ) upon its reduction by the conduction band electrons. However, further oxidation of these intermediates with another hydroxyl radical (or a valence band hole) leads to ring cleavage and therefore to noncyclic intermediates (Scheme 2.2).

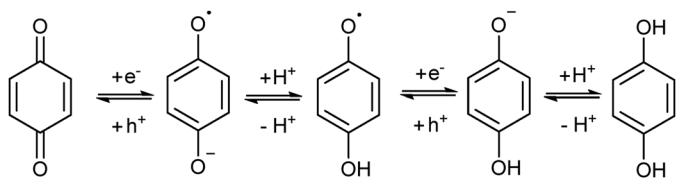

Scheme 2.1 Redox process hydroquinone–quinone as a sequence of proton and electron transfers.

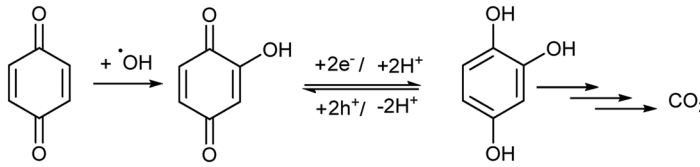

Scheme 2.2 Formation of hydroxybenzoquinone and its equilibrium with hydroxyhydroquinone.

Since these intermediates have been detected in the reaction media and not on the surface of the photocatalyst, it is not necessary for the oxidation form/reduction form (Ox/Red) equilibrium to occur on the surface of the same particle, meaning that the (Ox/Red) couple may transfer electrons from one particle to another in a mechanism similar to the Z-scheme mechanism.

Some inorganic systems can also behave as external recombination centers *via* the shuttle recombination mechanism. Examples of this are the Fe^{2+}/Fe^{3+} and Cu^{+}/Cu^{2+} couples.[41,42] In this case, the cations with lower oxidation states can be oxidized by the photogenerated valence band holes to the higher oxidation state cations. The thus formed cations can scavenge the conduction band electrons, resulting in the recombination of the photogenerated charge carriers according to eqn (2.21) and (2.22):

$$M^{n+} + h^{+}_{vb} \rightarrow M^{(n+1)+} \quad (2.21)$$

$$M^{(n+1)+} + e^{-}_{cb} \rightarrow M^{n+} \quad (2.22)$$

An inhibitory effect of ferric ions has been recognized during the study of the photocatalytic oxidation of methyl viologen in the presence of $FeCl_2$ which has been rationalized in terms of an "electron shuttle mechanism" involving the couple Fe^{2+}/Fe^{3+}.[41] Moreover, the presence of dissolved electron acceptors, *i.e.*, Fe^{3+} ions formed *via* the valence band oxidation of Fe^{2+}, suppresses the oxidation of the organic substrate to CO_2 *via* its competing reaction with molecular oxygen or by oxidizing the previously produced superoxide radicals.

2.4 Importance of the Reduction Pathway in Photocatalytic Oxidation Reactions

In the photocatalytic degradation of pollutants, UV(A)-illuminated TiO_2 has been successfully demonstrated as an active system for an immense number of substrates, which has been largely ascribed to the strong oxidation potential of the photogenerated valence band (VB) holes.[43] However, conduction band electrons may also participate in the photocatalytic degradation of a substrate either directly or through the formation of reactive oxygen species (ROS).

These ROS include $O_2^{\bullet -}$ or $HO_2^{\bullet}$, $^{\bullet}OH$ or $O^{\bullet -}$ radicals, H_2O_2, and $O_2\,^1$ or even O_3, $O_3^{\bullet -}$, $HO_4^{\bullet}$ and $HO_3^{\bullet}$ radicals.

As can be seen from Table 2.1 and Figure 2.1 the formation of all these ROS on illuminated TiO_2, for example, is thermodynamically possible. The formation of one or more of these ROS has clearly been confirmed during the decomposition of pollutants by specific techniques either in the gas phase or in the aqueous phase.[36,44–46] Interestingly, most of these ROS are produced *via* a reductive pathway rather than by an oxidative pathway in oxygenated photocatalytic systems meaning that the reduction power of the employed photocatalyst has also to be taken into account to achieve an efficient photocatalytic system. Figure 2.6 summarizes schematically the possible ROS formed in illuminated photocatalytic systems.

Although the formation of O_3, $O_3^{\bullet -}$, $HO_4^{\bullet}$, and $HO_3^{\bullet}$ has been largely unexplored, George and co-workers have reported a significant accumulation of O_3 during the photocatalytic degradation of NO on the surface of TiO_2.[47] They assumed that O_3 is formed *via* a surface chemical pathway involving the photochemistry of $^{\bullet}NO_3$ radicals which are produced *via* the charge exchange reaction between the nitrate anion and the solid surface. The formed $^{\bullet}NO_3$ radical can be photolyzed at longer wavelengths compared to the corresponding anion (NO_3^-), forming $O^{\bullet}$ atoms that react with molecular oxygen to produce O_3 as can be seen from eqn (2.23)–(2.26):

$$NO_3^- + h^+ \rightarrow NO_3^{\bullet} \tag{2.23}$$

$$NO_3^{\bullet} + h\nu \rightarrow NO_2 + O^{\bullet} \tag{2.24}$$

$$NO_3^{\bullet} + h\nu \rightarrow NO + O_2 \tag{2.25}$$

$$O^{\bullet} + O_2 + M \rightarrow O_3 + M \tag{2.26}$$

The reduction of ozone by hydrated electrons has been studied by Forni *et al.*[48] who reported a very high rate constant (3.6×10^{10} M^{-1} s^{-1}) for this reaction. The reaction between ozone and the conduction band electrons of the semiconductor is also thermodynamically possible (*cf.* Table 2.1), resulting in the formation of the ozonide radical anion (eqn (2.27)) which consequently leads to $HO^{\bullet}$ formation through reaction (eqn (2.28)):

$$O_3 + e^- \rightarrow O_3^{\bullet -} \tag{2.27}$$

$$O_3^{\bullet -} + H^+ \leftrightarrow HO_3^{\bullet} \rightarrow HO^{\bullet} + O_2 \tag{2.28}$$

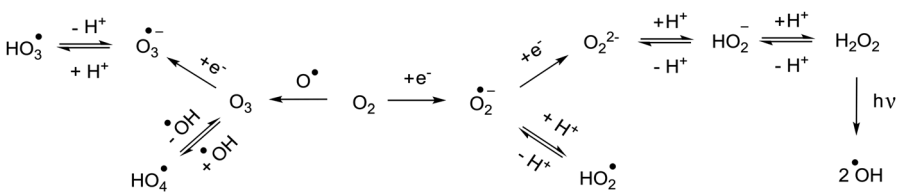

Figure 2.6 Photo(catalytically) formed reactive oxygen species.

Oxygen molecules will be reduced by the photogenerated conduction band electrons to form superoxide ($O_2^{\bullet -}$) or hydroperoxide radicals, respectively, as can be seen from the following reactions:

$$O_2 + e^- \rightarrow O_2^{\bullet -} \quad (2.29)$$

$$O_2^{\bullet -} + H^+ \leftrightarrow HO_2^{\bullet} \ (pK = 4.8) \quad (2.30)$$

Moreover, in the photocatalytic system, oxygen molecules may not only be reduced by the photogenerated conduction band electrons but they can also be attacked by organic radicals, which are formed *via* the reaction of the organic substrate with the valence band holes, resulting in the formation of organoperoxy radicals (eqn (2.31) and (2.32)):

$$RH + h^+ \rightarrow R^{\bullet} + H^+ \quad (2.31)$$

$$R^{\bullet} + O_2 \rightarrow ROO^{\bullet} \quad (2.32)$$

Schwitzgebel *et al.*[38] reported that the thus produced organoperoxy radical may react with superoxide $O_2^{\bullet -}$ or hydroperoxide radicals to form tetra-oxides that decompose to the respective final products:

$$ROO^{\bullet} + O_2^{\bullet -} \rightarrow ROOOO^- \quad (2.33)$$

$$ROO^{\bullet} + HOO^{\bullet} \rightarrow ROOOOH \quad (2.34)$$

Another possibility for the formation of the tetra-oxide is the so-called Russell reaction or Russell-like reaction, which are presented in Schemes 2.3 and 2.4, respectively.

Organoperoxides can also be produced *via* reduction of the organoperoxy radical followed by protonation. The thus formed organoperoxide may also react with the conduction band electrons to form hydroxide anions and alkoxy radicals (eqn (2.35)–(2.37)):

$$ROO^{\bullet} + e^- \rightarrow ROO^- \quad (2.35)$$

$$ROO^- + H^+ \rightarrow ROOH \quad (2.36)$$

$$ROOH + e^- \rightarrow RO^{\bullet} + OH^- \quad (2.37)$$

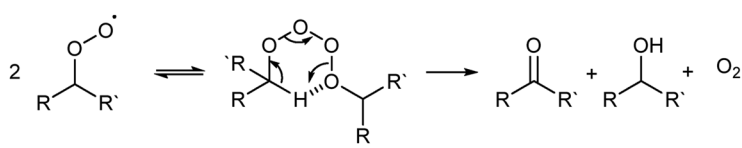

Scheme 2.3 Conversion of organoperoxy radical into alcohols and carbonyl compounds *via* the Russell reaction.

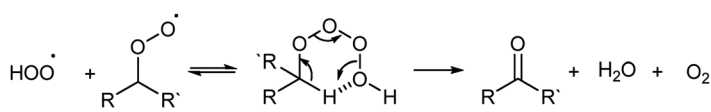

Scheme 2.4 Conversion of organoperoxy and hydroperoxy radicals into carbonyl compounds *via* a Russell-like reaction.

Organoperoxides have been detected beside H_2O_2 by Hoffmann and co-workers[46] upon the photocatalytic oxidation of acetate employing quantum-sized ZnO as photocatalysts. However, the authors mentioned that no organoperoxides were formed in the case of formate or oxalate since oxidation of these anions primarily leads to the formation of the $CO_2^{\bullet-}$ radical which is further oxidized to CO_2.

As a result, taking the reductive pathway into account, there will be fewer stages of oxidation of the organic molecules on their photocatalytic way to CO_2 and water.

Among various ROS, H_2O_2 is the most stable species, the conversion of which is closely coupled with other ROS. It serves as a reservoir species for more reactive ROS as well as a precursor of other ROS. Hydrogen peroxide (H_2O_2) can be photocatalytically generated on illuminated TiO_2 either *via* the reduction of O_2 or *via* the oxidation of H_2O. Likewise, H_2O_2 can be degraded on illuminated TiO_2 either oxidatively (eqn (2.15)–(2.17))[49] or reductively (eqn (2.40) and (2.41)):

$$O_2 + e^-_{CB} \rightarrow O_2^{\bullet-} \tag{2.38}$$

$$O_2^{\bullet-} + e^-_{CB} + 2H^+ \rightarrow H_2O_2 \tag{2.39}$$

$$H_2O_2 + e^-_{CB} \rightarrow OH^- + {}^{\bullet}OH \tag{2.40}$$

$$OH^- + {}^{\bullet}OH + e^-_{CB} + 2H^+ \rightarrow 2H_2O \tag{2.41}$$

Therefore, understanding these reactions occurring on the surface of irradiated TiO_2 should provide valuable information concerning the general mechanism of photocatalysis.

The photocatalytic decomposition of H_2O_2 may also generate $HO^{\bullet}$ and $HO_2^{\bullet}$ radicals; their production accompanied by the degradation of H_2O_2 was monitored in the gas phase immediately above the illuminated TiO_2 surface. Yi *et al.*[49] have studied the photocatalytic behavior of H_2O_2 on illuminated TiO_2 films using cavity ring down spectroscopy (CRDS), which enables an *in situ* monitoring of $HO_2^{\bullet}$ radicals as well as of H_2O_2 over the photocatalyst film. Their results indicate that the photocatalytic degradation of H_2O_2 occurs *via* $HO_2^{\bullet}$ radicals as intermediates initiated by its reaction with VB holes (see eqn (2.16)) but is also not retarded in the absence of O_2, implying that H_2O_2 itself also serves as an electron acceptor (see eqn (2.40)). The $HO_2^{\bullet}$ radical is a key intermediate of general photocatalytic reactions, and its fate should be critical in controlling the overall photocatalytic mechanism. Once it is formed, it may react with either a VB hole or with a CB electron (reactions 2.42 and 2.43), which should determine the overall mechanistic pathway:

$$HO_2^{\bullet}(ad) + {}^{\bullet}OH/h^+ \rightarrow O_2(ad) + H_2O/H^+ \tag{2.42}$$

$$HO_2^{\bullet}(ad) + e^- + H^+ \rightarrow H_2O_2(ad) \tag{2.43}$$

The fate of $HO_2^{\bullet}$, *i.e.*, generated from the decomposition of H_2O_2, has been found to be different among several TiO_2 films, which implies that the general photocatalytic reaction mechanism involving $HO_2^{\bullet}$ radicals depends on

the kind of TiO_2. On illuminated Evonik P25 TiO_2, for example, the *in situ* generated $HO_2^{\bullet}$ radicals are rapidly degraded with little chance of desorption into the surrounding atmosphere, while those formed over Aldrich anatase or Aldrich rutile films are long-lived enough to partially desorb into the surrounding atmosphere.[49]

Hoffmann and co-workers[46] have performed isotopic labeling experiments to elucidate the mechanism of peroxide production over illuminated ZnO, showing that the oxygen in the photoproduced hydrogen peroxide originates entirely from the oxygen gas according to reactions (2.44)–(2.46):

$$e_{CB}^- + O_2 \rightarrow O_2^{\bullet -} \tag{2.44}$$

$$2O_2^{\bullet -} \xrightarrow{2H^+} H_2O_2 + O_2 \tag{2.45}$$

$$O_2^{\bullet -} + e_{CB}^- + 2H^+ \rightarrow H_2O_2 \tag{2.46}$$

The photocatalytic degradation of nitro aromatic compounds employing TiO_2 follows reductive as well as oxidative pathways. Dillert *et al.*[50] have found that the photocatalytic activity for the degradation of nitro aromatic compounds decreases with an increasing number of nitro groups bound to the aromatic ring. In contrast, the presence of methyl groups at the aromatic ring enhanced the reactivity. The authors reported the following order of reactivity: nitrotoluenes > nitrobenzene > dinitrotoluenes > dinitrobenzenes > 2,4,6-trinitrotoluene > 1,3,5-trinitrobenzene. This order reflects the known influence of nitro groups towards the attack of an electrophilic reagent on the aromatic molecule. Two competitive pathways are suggested for the photocatalytic degradation of nitrotoluenes in the presence of TiO_2.[51] When the methyl group is the site of the initial attack it will be oxidized in subsequent steps to yield a carboxyl group that can be further converted into the corresponding nitrobenzenes after decarboxylation following a photo-Kolbe mechanism. However, the reaction pathway in the absence of methyl groups on the aromatic ring is more likely to occur through a reductive pathway in a mechanism involving sequential electron transfers, protonations, and dehydration (Scheme 2.5).

Nahen *et al.*[51] reported that the attack by reducing species is enhanced in the presence of hole scavengers such as methanol. In the presence of methanol, α-hydroxymethyl radicals will be formed that can either react with the

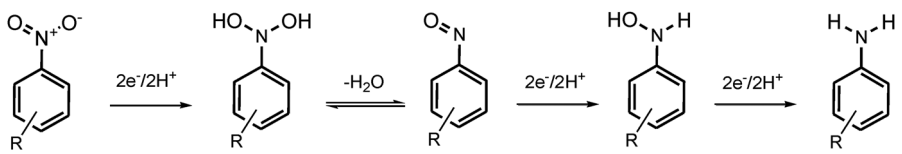

Scheme 2.5 Schematic illustration of the photocatalytic reduction of a nitroaromatic compound to an aminoaromatic compound.

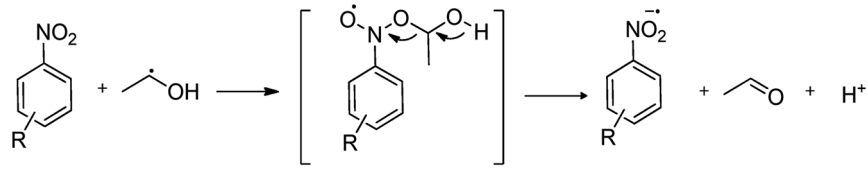

Scheme 2.6 Reduction of nitroaromatic compounds *via* their reaction with α-hydroxymethyl radicals.

nitro aromatic compound[52,53] (Scheme 2.6) or inject an electron into the valence band of the photocatalyst (current doubling effect; more details are given in Section 2.5).[54]

2.5 Importance of the Oxidation Pathway in Photocatalytic Reduction Reactions

Photocatalytic reduction reactions such as hydrogen generation from water or CO_2 reduction have been and are being very often performed in the presence of various organic and inorganic electron donors such as alcohols, organic acids, sulfide, and sulfite.[55] Since the oxidation of such compounds *via* photogenerated holes is very efficient, the charge–carrier recombination reaction can be suppressed, improving the reduction processes. However, the oxidation of such electron donors proceeds *via* the formation of intermediates that themselves may react with the educts, changing the hole reaction pathway. In many cases, the one-electron oxidation process results in the formation of strongly reducing radicals as intermediates, which can consequently participate in the reduction reaction. For instance, alcohol oxidation on the TiO_2 surface occurs *via* two reaction steps according to eqn (2.47)–(2.49) ($E_{1/2}$ values are taken from ref. 56): the first step includes the cleavage of the C–H bond resulting in the formation of the respective α-hydroxyalkyl radicals while the formation of the respective aldehyde occurs in the second step involving the injection of an electron into the conduction band of TiO_2, called "current doubling":[57–59]

$$CH_3OH \xleftarrow{E_{1/2}=0.72\,V} \dot{C}H_2OH + e^- \xleftarrow{E_{1/2}=-0.98\,V} CH_2O + e^-, \quad E_{1/2} = 1.7\,V \tag{2.47}$$

$$CH_3CH_2OH \xleftarrow{E_{1/2}=0.72\,V} CH_3\dot{C}HOH + e^- \xleftarrow{E_{1/2}=-1.18\,V} CH_3CHO + e^-, \quad E_{1/2} = 1.9\,V \tag{2.48}$$

$$(CH_3)_2CHOH \xleftarrow{E_{1/2}=0.9\,V} (CH_3)_2\dot{C}OH + e^- \xleftarrow{E_{1/2}=-1.3\,V} (CH_3)_2CO + e^-, \quad E_{1/2} = 2.2\,V \tag{2.49}$$

Morris *et al.*[60] proposed an overall photocatalytic oxidation mechanism of methanol on the surface of TiO_2 nanoparticles as depicted in Figure 2.7. Their

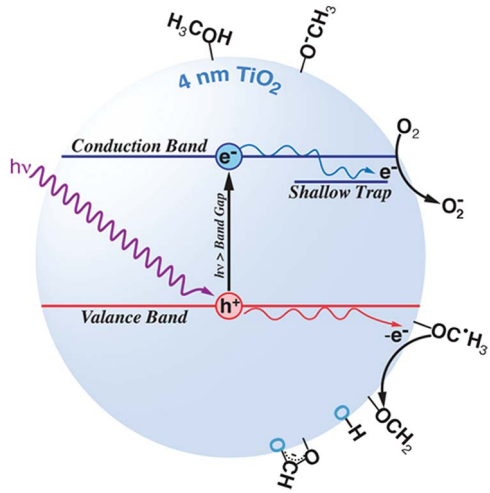

Figure 2.7 Photocatalytic oxidation mechanism of methanol on rutile TiO_2 nanoparticles in the presence of molecular oxygen. (Reprinted with permission from ref. 60. Copyright 2012 American Chemical Society.)

experimental data showed that methanol adsorbs predominantly *via* a dissociative pathway on the surface of 4 nm rutile nanoparticles to produce surface methoxy and hydroxyl groups. These surface methoxy groups serve as effective hole trapping centers. A two-electron transfer process involving the initial formation of a radical anion through the direct hole oxidation of the methanol molecule followed by a prompt electron injection from this radical anion into the TiO_2 conduction band is suggested (*i.e.*, the above-mentioned current-doubling process). Furthermore, the studies by Morris *et al.*[60] showed that the role of O_2 in promoting methanol photodecomposition is to scavenge free electrons, thus opening acceptor sites for the injection of new electrons during the methoxy group oxidation. In this way, O_2 increases the photonic efficiency by a factor of 5 without affecting the hole-mediated oxidation mechanism.

The reaction mechanism discussed above illustrates quite nicely that due to the current doubling effect at least half of the detected H_2 gas that is generated in a system containing alcohol as the sacrificial reagent is most likely formed through the action of holes and not of electrons in these so-called water splitting systems! Therefore, it is fair to say that the yields reported for the molecular hydrogen formation in such systems cannot (and should not!) be denoted as "water splitting efficiencies"! The same mechanisms are operative for many other electron donors such sulfide or sulfite as discussed by Schneider *et al.*[61]

The "current doubling effect" has been shown experimentally on TiO_2 photoanodes, whereupon an enhanced current in the presence of a sacrificial agent has been detected.[58] However, to our best knowledge, direct evidence for "current doubling" in the photocatalytic hydrogen generation process has not been shown yet, since this would mean the detection of a H_2 yield of 200%.

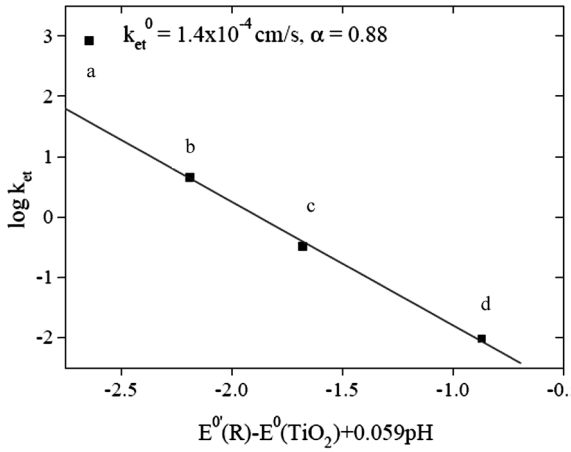

Figure 2.8 Interfacial electron transfer rate (k_{et}) for the reaction of TiO_2 with (a) e_{aq}^-, (b) H˙, (c) CH_3˙$COHCH_3$, and (d) ˙CH_2OH as function of driving force, which is defined as the difference between the standard redox potential of the reacting radicals, E°(R), and the potential of the excess conduction band electron, E° TiO_2. (Reprinted with permission from ref. 62. Copyright 2002 Elsevier Science Ltd.)

Nevertheless, Rabani *et al.*[62] have investigated the reaction of the α-hydroxyalkyl radicals formed upon the radiolysis of alcohols in acidic aqueous solutions at low pH in the presence of TiO_2 nanoparticles. According to their results the reactivity of these radicals with TiO_2 decreases in the order: e_{aq}^- > CH_3˙$COHCH_3$ > ˙CH_2OH, while the *t*-butanol radical is inert towards TiO_2, as expected. Moreover, with the exception of the methanol radical, the driving force for the electron injection process was found to be in the range −1.7 to −2.6 V, which is apparently within the Marcus (1965)[63] inverted range (Figure 2.8). Nevertheless, the reaction rate increases with the driving force as expected for a normal reaction. Note that these results are in contrast to the reported values for the electron transfer from the alcohol to the valence band of TiO_2. The reaction of photogenerated holes with the alcohols follows the order: CH_3OH > CH_3CH_2OH > $CH_3CHOHCH_2OH$.[64]

Since most photocatalytic reduction reactions are performed on semiconductors loaded with a co-catalyst such as Pt, Au, Rh, *etc.*, the electron injection from the radical anion into the co-catalyst followed by H^+ reduction has also to be considered. This would mean that the semiconductor simply participates in the oxidation process, providing strongly reducing radicals, while the reduction reaction occurs on the co-catalyst surface, which is not necessarily connected with a photocatalyst particle. According to Henglein *et al.*,[65] photocatalytically produced α-hydroxymethyl radicals were found to form molecular hydrogen in the presence of colloidal Pt, Au, Ag, and Cd. Conductivity measurements showed that electrons stored on the colloidal particles are intermediates of the H_2 formation. However, a recently published paper by Zidki *et al.*[66] contradicts these results, emphasizing that Pt nanoparticles do not catalyze the reduction of water in the presence of the

strongly reducing alcohol radicals. Not only due to this contradiction, it is worth studying such systems in more depth.

2.6 Conclusions

In summary, enhancement of the efficiency of the utilization of photogenerated charge carriers on the surface of photocatalysts requires greater understanding of the entire photocatalytic process. The reduction potentials of most substrates, as well as those of the intermediates formed during the photocatalytic reaction(s), are well known; nevertheless, it is essential to realize that thermodynamic properties may change upon the adsorption of these molecules at the photocatalyst surface. Therefore, a detailed understanding of the processes occurring on the photocatalyst surface before, during, and after light absorption is of utmost importance. On the other hand, the charge carriers generated upon light absorption that survive recombination and reach the semiconductor surface may suffer surface recombination processes or recombination *via* an electron shuttle mechanism (Z scheme deactivation mechanism), thus reducing the total efficiency of the photocatalytic system. Moreover, since the overall efficiency of a photocatalytic process will be determined by the efficiency of the slowest reaction step it is crucial to know whether this is the reductive or oxidative half-reactions. Besides the obvious one-electron transfer steps these reactions entail in particular multi-electron transfer processes, *e.g.*, the four-electron oxidation of water or the eight-electron reduction of CO_2. Hence, this chapter provides some necessary tools for the understanding and the development of the photocatalytic reaction mechanism.

References

1. R. v. d. Krol, in *Photoelectrochemical Hydrogen Production*, ed. R. v. d. Krol and M. Grätzel, Springer, US, 2012, vol. 102.
2. T. A. Kandiel, A. Feldhoff, L. Robben, R. Dillert and D. W. Bahnemann, *Chem. Mater.*, 2010, **22**, 2050.
3. H. Kato and A. Kudo, *J. Phys. Chem. B*, 2001, **105**, 4285.
4. M. A. Holmes, T. K. Townsend and F. E. Osterloh, *Chem. Commun.*, 2012, **48**, 371.
5. R. Memming, *Semiconductor Electrochemistry*, Wiley-VCH Verlag GmbH, Weinheim, 2001.
6. P. Wardman, *J. Phys. Chem. Ref. Data*, 1989, **18**, 1637.
7. S. N. Habisreutinger, L. Schmidt-Mende and J. K. Stolarczyk, *Angew. Chem., Int. Ed.*, 2013, **52**, 7372.
8. S. Y. Chen and L. W. Wang, *Chem. Mater.*, 2012, **24**, 3659.
9. V. V. Titov, R. V. Milchaylov and A. A. Lisachenko, *J. Phys. Chem. C*, 2012, **118**, 21986.
10. H. Courbon, M. Formenti and P. Pichat, *J. Phys. Chem.*, 1977, **81**, 550.

11. H. Courbon and P. Pichat, *C. R. Seances Acad. Sci., Ser. C*, 1977, **285**, 171.
12. J. Cunningham, E. L. Goold and J. L. G. Fierro, *J. Chem. Soc., Faraday Trans. 1*, 1982, **78**, 785.
13. S. Sato, *J. Phys. Chem.*, 1987, **91**, 2895.
14. S. Sato and T. Kadowaki, *J. Catal.*, 1987, **106**, 295.
15. S. Sato, T. Kadowaki and K. Yamaguti, *J. Phys. Chem.*, 1984, **88**, 2930.
16. J. F. Montoya, I. Ivanova, R. Dillert, D. W. Bahnemann, P. Salvador and J. Peral, *J. Phys. Chem. Lett.*, 2013, **4**, 1415.
17. J. F. Montoya, D. W. Bahnemann, J. Peral and P. Salvador, *ChemPhysChem.*, 2014, **15**, 2311.
18. J. Schneider, M. Matsuoka, M. Takeuchi, J. Zhang, Y. Horiuchi, M. Anpo and D. W. Bahnemann, *Chem. Rev.*, 2014, **114**, 9919.
19. C. Kormann, D. W. Bahnemann and M. R. Hoffmann, *J. Phys. Chem.*, 1988, **92**, 5196.
20. A. J. Hoffman, H. Yee, G. Mills and M. R. Hoffmann, *J. Phys. Chem.*, 1992, **96**, 5540.
21. G. K. Ramesha, J. F. Brennecke and P. V. Kamat, *ACS Catal.*, 2014, **4**, 3249.
22. H. Y. He, P. Zapol and L. A. Curtiss, *J. Phys. Chem. C*, 2010, **114**, 21474.
23. K. Bhattacharyya, A. Danon, B. K. Vijayan, K. A. Gray, P. C. Stair and E. Weitz, *J. Phys. Chem. C*, 2013, **117**, 12661.
24. O. Tomita, B. Ohtani and R. Abe, *Catal. Sci. Technol.*, 2014, **4**, 3850.
25. R. F. Howe and M. Grätzel, *J. Phys. Chem.*, 1987, **91**, 3906.
26. T. Berger, M. Sterrer, O. Diwald, E. Knozinger, D. Panayotov, T. L. Thompson and J. T. Yates, *J. Phys. Chem. B*, 2005, **109**, 6061.
27. O. I. Micic, Y. N. Zhang, K. R. Cromack, A. D. Trifunac and M. C. Thurnauer, *J. Phys. Chem.*, 1993, **97**, 7277.
28. K. Ishibashi, A. Fujishima, T. Watanabe and K. Hashimoto, *J. Photochem. Photobiol. A*, 2000, **134**, 139.
29. A. Imanishi, T. Okamura, N. Ohashi, R. Nakamura and Y. Nakato, *J. Am. Chem. Soc.*, 2007, **129**, 11569.
30. P. Delahay and K. Vonburg, *Chem. Phys. Lett.*, 1981, **83**, 250.
31. R. Nakamura and Y. Nakato, *J. Am. Chem. Soc.*, 2004, **126**, 1290.
32. P. Salvador, *Prog. Surf. Sci.*, 2011, **86**, 41.
33. J. Freitag, A. DomÃnguez, T. A. Niehaus, A. Hälsewig, R. Dillert, T. Frauenheim and D. W. Bahnemann, *J. Phys. Chem. C*, 2015, **119**, 4488.
34. T. Rajh, L. X. Chen, K. Lukas, T. Liu, M. C. Thurnauer and D. M. Tiede, *J. Phys. Chem. B*, 2002, **106**, 10543.
35. G. Zhang, G. Kim and W. Choi, *Energy Environ. Sci.*, 2014, **7**, 954.
36. M. Mrowetz and E. Selli, *New J. Chem.*, 2006, **30**, 108.
37. Y. Wang and P. Y. Zhang, *J. Hazard. Mater.*, 2011, **192**, 1869.
38. J. Schwitzgebel, J. G. Ekerdt, H. Gerischer and A. Heller, *J. Phys. Chem.*, 1995, **99**, 5633.
39. J. Theurich, M. Lindner and D. W. Bahnemann, *Langmuir*, 1996, **12**, 6368.
40. C. Richard, *New J. Chem.*, 1994, **18**, 443.
41. D. W. Bahnemann, C. H. Fischer, E. Janata and A. Henglein, *J. Chem. Soc., Faraday Trans. 1*, 1987, **83**, 2559.

42. X. Chen, L. Liu, Z. Liu, M. A. Marcus, W.-C. Wang, N. A. Oyler, M. E. Grass, B. Mao, P.-A. Glans, P. Y. Yu, J. Guo and S. S. Mao, *Sci. Rep.*, 2013, **3**, 1510.
43. M. R. Hoffmann, S. T. Martin, W. Y. Choi and D. W. Bahnemann, *Chem. Rev.*, 1995, **95**, 69.
44. M. N. Romanias, A. El Zein and Y. Bedjanian, *J. Phys. Chem. A*, 2012, **116**, 8191.
45. L. F. Yin, J. F. Niu, Z. Y. Shen and J. Chen, *Environ. Sci. Technol.*, 2010, **44**, 5581.
46. A. J. Hoffman, E. R. Carraway and M. R. Hoffmann, *Environ. Sci. Technol.*, 1994, **28**, 776.
47. M. E. Monge, C. George, B. D'Anna, J. F. Doussin, A. Jammoul, J. Wang, G. Eyglunent, G. Solignac, V. Daele and A. Mellouki, *J. Am. Chem. Soc.*, 2010, **132**, 8234.
48. L. Forni, D. Bahnemann and E. J. Hart, *J. Phys. Chem.*, 1982, **86**, 255.
49. J. Yi, C. Bahrini, C. Schoemaecker, C. Fittschen and W. Choi, *J. Phys. Chem. C*, 2012, **116**, 10090.
50. R. Dillert, M. Brandt, I. Fornefett, U. Siebers and D. Bahnemann, *Chemosphere*, 1995, **30**, 2333.
51. M. Nahen, D. Bahnemann, R. Dillert and G. Fels, *J. Photochem. Photobiol., A*, 1997, **110**, 191.
52. J. L. Ferry and W. H. Glaze, *Langmuir*, 1998, **14**, 3551.
53. A. Hakki, R. Dillert and D. W. Bahnemann, *Phys. Chem. Chem. Phys.*, 2013, **15**, 2992.
54. M. Miyake, H. Yoneyama and H. Tamura, *Chem. Lett.*, 1976, 635.
55. X. B. Chen, S. H. Shen, L. J. Guo and S. S. Mao, *Chem. Rev.*, 2010, **110**, 6503.
56. J. Lilie, G. Beck and A. Henglein, *Ber. Bunsenges. Phys. Chem.*, 1971, **75**, 458.
57. R. Memming, Photoinduced charge transfer processes at semiconductor electrodes and particles, in *Electron Transfer 1*, ed. J. Mattay, Springer-Verlag, Berlin Heidelberg, 1994, Topics in Current Chemistry, vol. 169, pp. 105–181.
58. N. Hykaway, W. M. Sears, H. Morisaki and S. R. Morrison, *J. Phys. Chem.*, 1986, **90**, 6663.
59. S. Nakabayashi, S. Komuro, Y. Aoyagi and A. Kira, *J. Phys. Chem.*, 1987, **91**, 1696.
60. D. A. Panayotov, S. P. Burrows and J. R. Morris, *J. Phys. Chem. C*, 2012, **116**, 6623.
61. J. Schneider and D. W. Bahnemann, *J. Phys. Chem. Lett.*, 2013, **4**, 3479.
62. R. M. Gao, A. Safrany and J. Rabani, *Radiat. Phys. Chem.*, 2002, **65**, 599.
63. R. A. Marcus, *J. Chem. Phys.*, 1965, **43**, 679.
64. Y. Tamaki, A. Furube, M. Murai, K. Hara, R. Katoh and M. Tachiya, *J. Am. Chem. Soc.*, 2006, **128**, 416.
65. A. Henglein, B. Lindig and J. Westerhausen, *J. Phys. Chem.*, 1981, **85**, 1627.
66. T. Zidki, R. Bar-Ziv, U. Green, H. Cohen, D. Meisel and D. Meyerstein, *Phys. Chem. Chem. Phys.*, 2014, **16**, 15422.